K. Wang, Y. Yu, A.-C. Wong, and C. T.-C. Nguyen, "VHF free-free beam high-*Q* micromechanical resonators," *Technical Digest*, 12th International IEEE Micro Electro Mechanical Systems Conference, Orlando, Florida, Jan. 17-21, 1999, pp. 453-458.

VHF Free-Free Beam High-*Q* Micromechanical Resonators

Kun Wang, Yinglei Yu, Ark-Chew Wong, and Clark T.-C. Nguyen

Center for Integrated Microsystems
Department of Electrical Engineering and Computer Science
University of Michigan
Ann Arbor, Michigan 48109-2122

ABSTRACT

Free-free beam, flexural-mode, micromechanical resonators utilizing non-intrusive supports to achieve measured *Q*'s as high as 8,400 at VHF frequencies from 30-90MHz are demonstrated in a polysilicon surface micromachining technology. The subject microresonators feature torsional-mode support springs that effectively isolate the resonator beam from its anchors via quarter-wavelength impedance transformations, minimizing anchor dissipation and allowing these resonators to achieve high *Q* with high stiffness in the VHF frequency range.

I. INTRODUCTION

Vibrating beam micromechanical (or "μmechanical") resonators constructed in a variety of materials, from polycrystalline silicon to plated-nickel, have recently emerged as potential candidates for use in a variety of frequency-selective communications applications [1]. In particular, provided the needed VHF and UHF frequencies can be attained, both low loss IF and RF filters and high-*Q* oscillators stand to benefit from the tiny size, virtually zero dc power consumption, and integrability of such devices.

To date, due to the relative ease with which they attain both small mass and high stiffness, clamped-clamped beam μmechanical resonators have been intensively investigated for VHF range applications [2-3]. The ability to simultaneously achieve high *Q* and high stiffness is paramount for communications-grade resonators, since stiffness directly influences the dynamic range of circuits comprised of such resonators [4]. However, for the case of clamped-clamped beam designs, larger stiffness often comes at the cost of increased anchor dissipation, and thus, lower resonator *Q*. This work attempts to address the problem by retaining the basic flexural-mode beam design of previous resonators, but strategically altering their supports so that anchors and their associated losses are virtually eliminated from the design. Using this approach, free-free beam μmechanical resonators are demonstrated with center frequencies from 30MHz to 90MHz, high stiffnesses, and *Q*'s as high as 8,400.

II. RESONATOR STRUCTURE AND OPERATION

Figure1 presents the scanning electron micrograph (SEM) of the prototype, 70MHz, free-free beam, flexural-mode, μmechanical resonator of this work, indicating various components

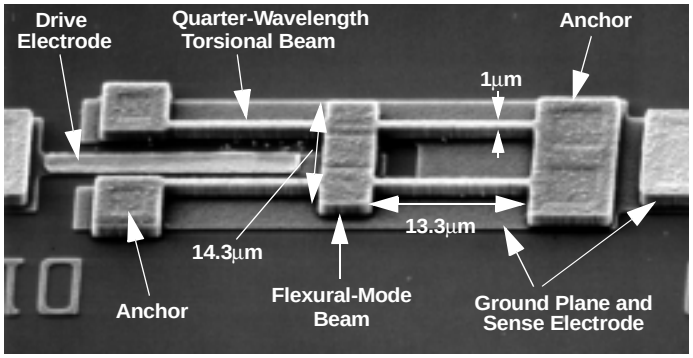

Fig. 1: SEM of a 70.95MHz free-free beam μmechanical resonator.

and dimensions. For enhanced clarity, Fig. 2 presents a perspective-view schematic of this resonator, providing additional details and specifying a preferred electrical pickoff scheme.

As shown, this device is comprised of a free-free μmechanical beam supported at its flexural node points by four torsional beams, each of which is anchored to the substrate by rigid contact anchors. An electrode is provided underneath the free-free beam to allow electrostatic excitation via an applied ac voltage v_i, and output currents are detected directly off the dc-biased (via V_P) resonator structure. The torsional support beams for this device are strategically designed with quarter-wavelength dimensions, so as to affect an impedance transformation that isolates the free-free beam from the rigid anchors. Ideally, the free-free beam sees zero-impedance into its supports, and thus, effectively operates as if levitated without any supports. As a result, anchor dissipation mechanisms normally found in previous clamped-clamped beam resonators are greatly suppressed, allowing much higher device *Q*.

As an additional yield- and *Q*-enhancing feature, the transducer capacitor gap spacing in this device is no longer entirely determined via a thin sacrificial oxide, as was done (with difficulty) in previous clamped-clamped beam high frequency devices [1,3]. Rather, the capacitor gap is now determined by the height of a dimple, set via a timed etch. As shown in Fig. 3, the height of the dimple is such that when a sufficiently large dc-bias V_P is applied between the electrode and resonator, the whole structure comes down and rests upon the dimples, which are located at flexural node points, and thus, have little impact

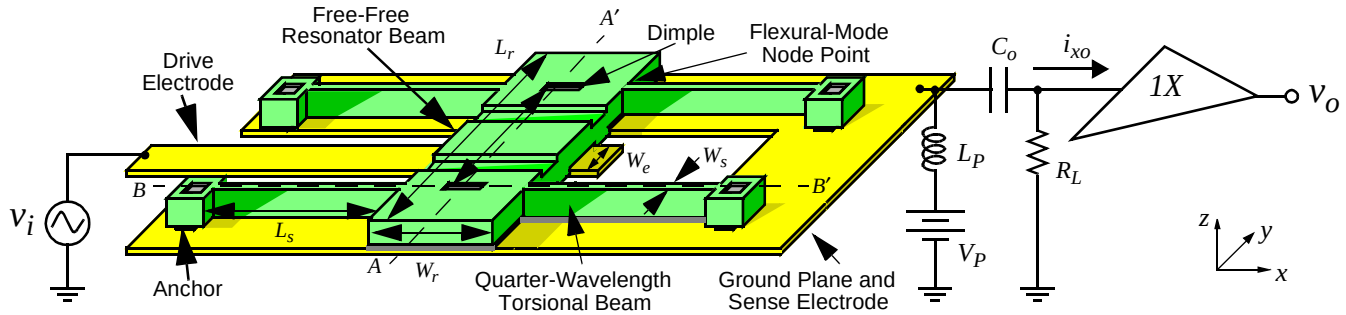

Fig. 2: Perspective-view schematic of the free-free beam resonator with non-intrusive supports, explicitly indicating important features and specifying a typical bias, excitation, and off-chip output sensing configuration.

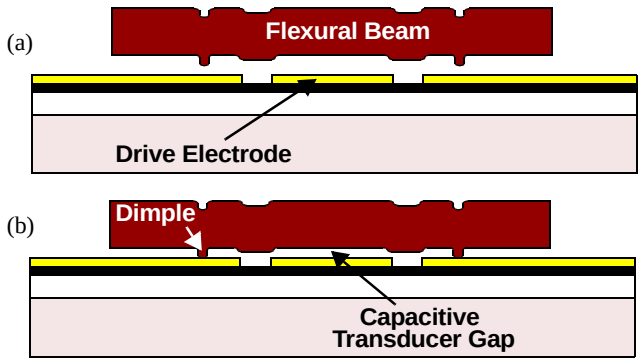

Fig. 3: Cross-sections (along *AA′* in Fig. 2) summarizing the electrostatically activated capacitor gap feature of this design. (a) Immediately after fabrication. (b) After application of an appropriately sized dc-bias voltage V_d.

on resonator operation. The advantages of using dimples to set the capacitor gap spacings are two-fold: (1) much thicker sacrificial oxide spacers can now be used, alleviating previous problems due to pinholes and non-uniformity in ultra-thin sacrificial layers; and (2) the thicker sacrificial oxide is easier to remove than previous thinner ones, and thus, decreases the required HF release etch time and lessens the chance that etch by-products remain in the gap (where they might interfere with resonator operation and *Q* [1,3]).

III. FREE-FREE BEAM μRESONATOR DESIGN

Proper design of the subject free-free beam μmechanical resonator entails not only the selection of geometries that yield a given frequency, but also geometries that insure support isolation, that guarantee dimple-down and pull-in stability, and that suppress spurious modes associated with the more complicated support network. Each of these topics is now addressed.

Resonator Beam Design.

For most practical designs, the resonator beam width W_r is dictated by transducer and length-to-width ratio design considerations, while its thickness h is determined primarily by process constraints. Almost by default, then, the length L_r becomes the main variable with which to set the overall resonance frequency. For the case of a large L_r-to-W_r ratio, the popular Euler-Bernoulli equation for the fundamental mode frequency of a free-free beam suffices, given by [5]

$$f_o = \frac{1}{2\pi}\alpha\sqrt{\frac{k_{ri}}{m_{ri}}} = \frac{1}{2\pi}\alpha\sqrt{\frac{k_{mi}}{m_{ri}}}\left(1-\left\langle\frac{k_e}{k_m}\right\rangle\right)^{1/2} \quad (1)$$

where k_{ri} and m_{ri} are the effective stiffness and mass, respectively, at the midpoint of the μresonator beam; α is a fitting parameter that accounts for beam topography and finite elasticity in the anchors; k_{mi} is the *mechanical* stiffness of the μresonator, again, at the midpoint of the beam, but this time for the special case when V_P=0V and given by

$$k_{mi} = \left[1.03\sqrt{\frac{E}{\rho}}\frac{h}{L_r^2}\right]^2 m_{ri}; \quad (2)$$

and $\langle k_e/k_m\rangle$ is a parameter representing the combined mechanical-to-electrical stiffness ratios integrated over the electrode width W_e, and satisfying the relation:

$$\left\langle\frac{k_e}{k_m}\right\rangle = \int_{\frac{1}{2}(L_r-W_e)}^{\frac{1}{2}(L_r+W_e)} \frac{V_P^2\varepsilon_o W_r}{d^3 k_m(y')}dy' \quad (3)$$

where ε_o is the permittivity in vacuum, d is the electrode-to-resonator gap spacing with dimples down, all other geometric variables are given in Fig. 2, and the location dependence of the mechanical stiffness k_m is now shown explicitly [4].

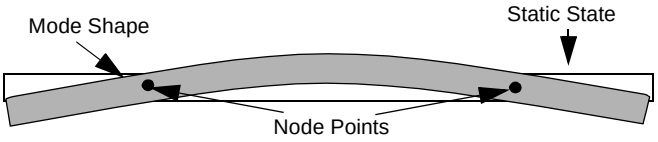

Fig. 4: The free-free beam mode shape.

Equation (1) constitutes a convenient closed form relation that works well for low frequency designs, where beam lengths are much larger than their corresponding widths and thicknesses. For upper VHF designs, for which beam lengths begin to approach their width and thickness dimensions, the Euler-Bernoulli equation is no longer accurate, since it ignores shear displacements and rotary inertias. To obtain accurate beam lengths for upper VHF μmechanical resonators, the design procedure by Timoshenko is more appropriate [5], involving the simultaneous solution of the coupled equations

$$\frac{d}{dy}\left(EI_r\frac{d\psi}{dy}\right)+\kappa AG\left(\frac{dz}{dy}-\Psi\right)-J_r\frac{d^2\Psi}{dt^2} = 0 \quad (4)$$

$$m\frac{d^2z}{dt^2}-\frac{d}{dy}\left[\kappa AG\left(\frac{dz}{dy}-\Psi\right)\right]-p(y,t) = 0 \quad (5)$$

where

$$I_r = \frac{W_r h^3}{12},\ G = \frac{E}{2(1+\nu)},\ \text{and}\ J_r = hW_r\frac{(h^2+W_r^2)}{12}, \quad (6)$$

and where I_r is the moment of inertia, E is the Young's modulus of the structural material, ν is Poisson's ratio, κ is a shape factor (for a rectangular cross section, κ is 2/3), A, m, and $p(y,t)$ are the cross-sectional area, mass per unit length, and loading per unit length, respectively, of the beam, Ψ is the slope due to bending, and axis definitions are provided in Fig. 2.

Support Structure Design.

As discussed in Section II, the subject free-free μmechanical resonator is supported by four torsional beams attached at its fundamental-mode node points, identified in Fig. 4 and specified via evaluation of the mode shape equation:

$$Z_{mode}(y) = \cosh\beta y+\cos\beta y-\zeta[\sinh\beta y+\sin\beta y], \quad (7)$$

where

$$\zeta = \frac{\cosh\beta L_r-\cos\beta L_r}{\sinh\beta L_r-\sin\beta L_r}\ \text{and}\ \beta^4 = \frac{\rho A}{EI_r}\omega_o^2, \quad (8)$$

and where ω_o is the radian resonance frequency, and ρ is the density of the structural material. For the fundamental mode, βL_r is 4.73.

Because they are attached at node points, the support springs (ideally) sustain no translational movement during resonator vibration, and thus, support (i.e., anchor) losses due to translational movements—such as those sustained by clamped-clamped beam resonators—are greatly alleviated. Furthermore, with the recognition that the supporting torsional beams actually behave like acoustic transmission lines at the VHF frequencies of interest, torsional loss mechanisms can also be negated by strategically choosing support dimensions so that they present virtually no impedance to the free-free beam. In particular, by choosing the dimensions of a torsional support beam such that they correspond to an effective quarter-wavelength of the resonator operating frequency, the solid anchor condition on one side

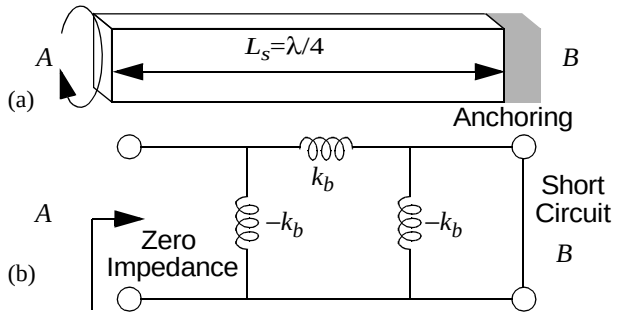

Fig. 5: (a) Quarter-wavelength torsional beam with *B* side anchoring; (b) Equivalent acoustic network showing zero impedance at port *A* with port *B* grounded.

of the support beam is transformed to a free end condition on the other side, which connects to the resonator. As a result, the resonator effectively "sees" no supports at all and operates as if levitated above the substrate, devoid of anchors and their associated loss mechanisms.

The above transformation is perhaps more readily seen using the equivalent acoustic π network model for a torsional beam. In particular, when the dimensions of a given support beam correspond to an effective quarter-wavelength of the resonator operation frequency, its equivalent acoustic π network takes the form shown in Fig. 5(b), where series and shunt arm impedances are modeled by equal and opposite stiffnesses, k_b and $-k_b$. Given that anchoring the beam of Fig. 5(a) at side *B* corresponds to shorting the *B* port of Fig. 5(b), it is clear by cancellation of the remaining k_b and $-k_b$ in the circuit of Fig. 5(b) that the impedance seen at port *A* will be zero.

Through appropriate acoustical network analysis, the dimensions of a torsional beam are found to correspond to a quarter wavelength of the operating frequency when they satisfy the expression

$$L_s = \frac{1}{4f_o}\sqrt{\frac{G\gamma}{\rho J_s}}, \tag{9}$$

where the subscript *s* denotes a support beam, J_s=J_r, and γ is the torsional constant [6].

Transducer Design.

The value of the series motional resistance R_z (among other impedance elements) seen looking into the input electrode of a μmechanical resonator is of utmost importance in both filtering and oscillator applications [1,4]. As with previous capacitively transduced clamped-clamped beam μmechanical resonators, parameters such as W_e, W_r, and *d*, that directly influence the electrode-to-resonator overlap capacitance have a direct bearing on the electrical impedance seen looking into the input electrode, as does the dc-bias V_P applied to the resonator. By appropriate impedance analysis, the expression governing R_z for this capacitively transduced free-free beam μmechanical resonator takes on the form

$$R_z = \frac{V_i}{I_z} = \left[\int_{L_1}^{L_2}\int_{L_1}^{L_2} \frac{\omega_o Q V_P^2(\varepsilon_o W_r)^2}{d^4 k_m(y')} \frac{Z_{mode}(y)}{Z_{mode}(y')} dy'dy\right]^{-1}, \tag{10}$$

where $L_1 = 0.5(L_r - W_e)$ and $L_2 = 0.5(L_r + W_e)$ for a centered electrode.

As discussed in Section II, under normal operation the free-free beam resonator must be pulled down onto its supporting dimples via a dc-bias voltage V_P applied to the resonator. Only when the dimples are "down" is the electrode-to-resonator gap spacing *d* small enough to provide adequate electromechanical coupling for most applications. Thus, when designing the device input electrode, careful consideration must be given to not only the input impedance seen when looking into the electrode, but also to the V_P required to pull the dimples down. This V_P voltage should be sufficient to pull the resonator down onto its dimples, yet small enough to avoid further pull-down of the free-free beam into the electrode after the dimples are down. Symbolically, the dc-bias voltage V_P must satisfy the relation

$$V_c > V_P > V_d\,, \tag{11}$$

where V_d is the dimple-down voltage, and V_c is the catastrophic resonator pull-down voltage.

When pulling the resonator down onto its dimples, because the supporting beams are often much more compliant than the free-free resonator beam, very little bending occurs in the resonator itself. Thus, the restoring force inhibiting pull-down is uniform over the electrode, and the expression for the dimple-down voltage V_d takes on the form [7]

$$V_d = \sqrt{\frac{8}{27}\frac{k_s d_{ini}^3}{\varepsilon_o W_r W_e}} \quad , \quad \text{where } k_s = EW_s\left(\frac{h}{L_s}\right)^3 \tag{12}$$

where k_s is the stiffness of supporting beams, and d_{ini} is the initial gap before the beam is brought down to its dimples.

Once the dimples are down, further movement of the resonator beam towards the electrode is attained via bending of the resonator itself. The electrode now sees a distributed stiffness inhibiting pull-down, which now must be integrated over the electrode area to accurately predict the catastrophic resonator pull-down voltage V_c. The procedure for determining V_c then amounts to setting (3) equal to 1 and solving for the V_P variable.

Table I: Euler & Timoshenko Design Comparison

Parameter	Euler Beam	Timoshenko Beam	Unit
Designed Frequency, f_o	70	70	MHz
Measured Frequency, f_o	66.62	70.94	MHz
Resonator Beam Length, L_r	15.4	14.9	μm
Resonator Beam Width, W_r	6	6	μm
Supporting Beam Length, L_s	13.4	13.3	μm
Supporting Beam Width, W_s	1	1	μm
Resonator Stiffness, k_{ri}	55,638	53,901	N/m
Resonator Mass, m_{ri}	$2.88\text{x}10^{-13}$	$2.79\text{x}10^{-13}$	kg
Initial Gap, d_{ini}	1,500	1,500	Å
Dimple Height, *d*	1,000	1,000	Å
Dimple-Down Voltage, V_d	98	98	V
Catastrophic Pull-In Voltage, V_c	255.9	268.9	V
Young's Modulus, *E*	150	150	GPa
Poisson Ratio, ν	0.29	0.29	—

IV. FABRICATION

Several free-free beam μresonators with frequencies from 30-90MHz and with varying initial gaps and dimple depths were designed using the methods detailed in Section III, then fabricated using a five-mask, polysilicon, surface-micromachining technology described by the process flow shown in Fig. 6. Table I summarizes design data for a 70MHz version, with reference to the parameters and dimensions indicated in Fig. 2.

The fabrication sequence begins with isolation layers formed via successive growth and deposition of 2μm thermal oxide and 2000Å LPCVD Si_3N_4, respectively, over a <100> lightly-doped

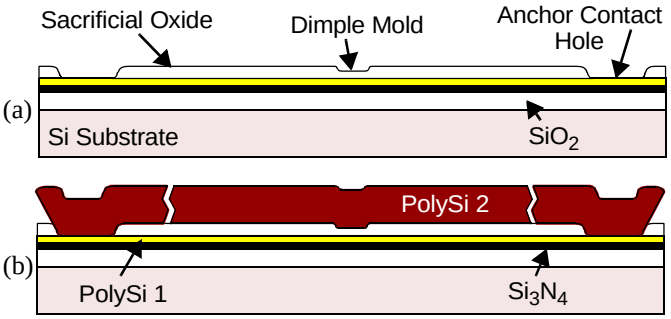

Fig. 6: Free-free μmechanical beam fabrication process flow, with cross-sections taken along *BB′* in Fig. 2.

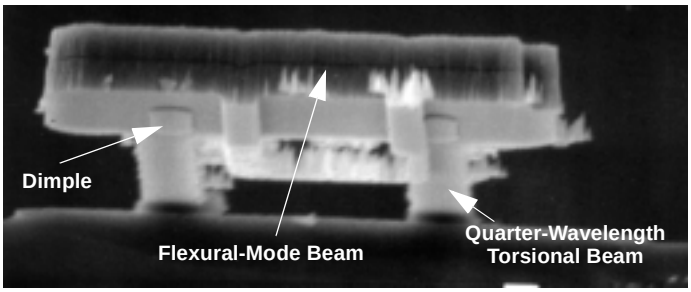

Fig. 7: Underside SEM of a free-free beam design, explicitly showing the supporting dimples.

p-type starting silicon wafer. Next, 3000Å of LPCVD polysilicon is deposited at 585°C and phosphorous-doped via implantation, then patterned to form ground planes and interconnects. An LPCVD sacrificial oxide layer is then deposited to a thickness dictated by (12), after which successive masking steps are used to achieve dimples and anchor openings (c.f., Fig.6(a)). To insure accurate depths, dimples are defined via a precisely controlled reactive-ion etch using a CF_4 chemistry. Anchors, on the other hand, are simply wet-etched in a solution of buffered hydrofluoric acid (BHF).

Next, the structural polysilicon is deposited via LPCVD at 585°C, and phosphorous dopants are introduced via ion-implantation. A 2000Å-thick oxide mask is then deposited via LPCVD at 900°C, after which wafers are annealed for one hour at 1000°C to relieve stress and distribute dopants. Both the oxide mask and structural layer are then patterned via SF_6/O_2- and Cl_2-based RIE etches, respectively, and structures are then released via a 5 minute etch in 48.8 wt. % HF. Note that this release etch time is significantly shorter than that required for previous clamped-clamped beam resonators (~1 hr) that did not benefit from dimple-activated gap spacings, and so required sacrificial oxide thicknesses on the order of hundreds of Angstroms.

After structural release, aluminum is evaporated and patterned over polysilicon interconnects via lift-off to reduce series resistance. An SEM showing the underside of this resonator (obtained via a fortunate wafer cleaving) is shown in Fig. 7, where the supporting dimples are clearly shown.

V. EXPERIMENTAL RESULTS

A custom-built vacuum chamber with pc board support and electrical feedthroughs allowing coaxial and dc connections to external instrumentation was utilized to characterize free-free μmechanical resonators, as well as clamped-clamped versions [2] and even folded-beam, comb-transduced lateral resonators [8] that were included in this run for comparative purposes. In this apparatus, devices under test were epoxied to a custom-built pc board containing surface-mounted detection electronics, and data was collected using an HP 4195A Network/Spectrum Analyzer. A turbomolecular pump was used to evacuate the chamber

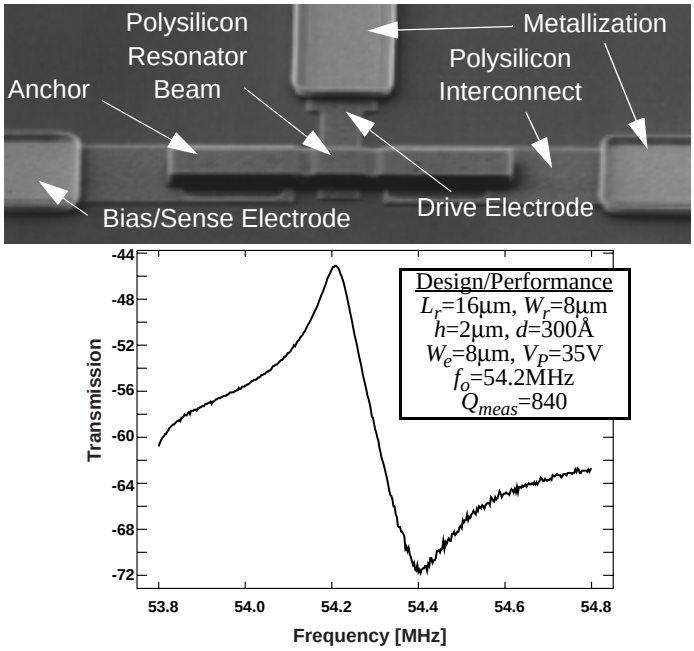

Fig. 8: SEM and measured frequency spectrum for a 54.2MHz clamped-clamped beam μmechanical resonator.

to pressures on the order of 50μTorr (which removes viscous gas damping mechanisms [9]) before testing devices.

To assess the overall quality of the polysilicon attained, 400kHz folded-beam μmechanical resonators were tested first using previously documented methods [10]. The *Q* of these resonators had an average value of about 12,000—much lower than the 50,000 of previous runs [10,11], indicating suboptimal polysilicon material in this particular run. Although lower than desired, this *Q* still proved sufficient for the present clamped-clamped versus free-free beam comparison.

Clamped-clamped beam μmechanical resonators were tested next using the above apparatus along with the motional current detection scheme shown in Fig. 2. Figure 8 presents the SEM and measured frequency characteristic for a 54.2 MHz clamped-clamped beam resonator operated under 50 μTorr vacuum. The directly measured *Q* of this device, with 180Ω of interconnect series resistance R_p included, is 840. Using a calculated value of series motional resistance R_z=4kΩ to account for loading by R_p, the actual resonator *Q* is found to be about 900.

The frequency characteristic for a 50.3MHz free-free beam μmechanical resonator was then obtained under identical conditions. Figure 9 presents the measured result, clearly showing a substantially higher *Q*, with a directly measured value of 8,430, and an extracted value of 8,673 when accounting for 400Ω of interconnect series resistance loading the resonator R_z=9.7kΩ. Even greater *Q* discrepancies are observed in Figs.10(a) and (b), which compare measured spectra for clamped-clamped and free-free beam μmechanical resonators around 70MHz, showing a *Q* difference as large as 28X at this frequency.

Given that the devices yielding Figs. 8-9 and 10(a)-(b) differ in only their end conditions (i.e., their anchoring methods), these data strongly suggest that anchor dissipation becomes a dominant loss mechanism for clamped-clamped beam resonators with high stiffness at VHF frequencies, and that the use of free-free beam resonators with non-intrusive supports can greatly alleviate this loss mechanism.

In addition, the data in Figs. 8 and 10(a) also show that clamped-clamped beam resonators exhibit a lowering in *Q* as frequencies increase from 50-70MHz, whereas their free-free beam counterparts maintain a fairly constant *Q* over this range.

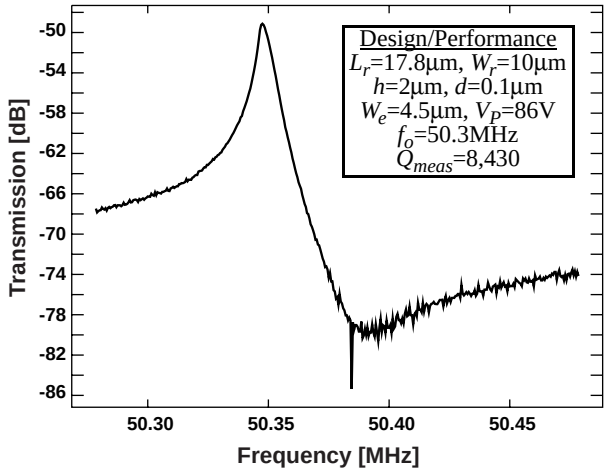

Fig. 9: Measured frequency spectrum for a 50.3MHz free-free beam μmechanical resonator.

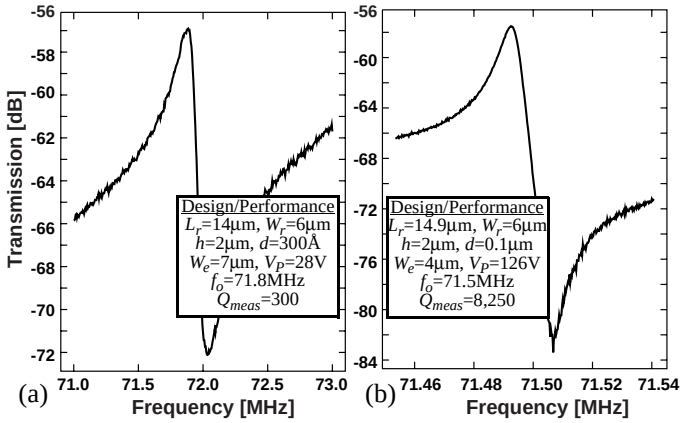

Fig. 10: Measured frequency spectra for (a) a 71.8MHz clamped-clamped beam μresonator; and (b) a 71.5MHz free-free beam μresonator.

These results further support an anchor-derived loss model for clamped-clamped beam resonators, where the stiffer the beam (i.e., the higher frequency, as dictated by (1)), the larger the force per cycle exerted on the substrate by anchors, therefore, the larger the energy loss per cycle, and the lower the Q. Under this model, the free-free beam resonators of this work, which (ideally) have no anchors, should exhibit Q's largely independent of frequency, at least in this VHF range. In this respect, Figs. 9 and 10(b) are certainly consistent with an anchor-dominated dissipation model, as are additional data at 31.51MHz and 92.25MHz shown in Figs. 11(a) and (b), respectively.

Small Length Effects.

Among resonators designed using Euler or Timoshenko methods, the latter were clearly closer to their target frequencies. In particular, as presented in Table I, fabricated μresonators designed using Timoshenko theory were fairly close to the desired frequency, while those designed using Euler-Bernoulli methods were as much as 4.8% too low. Evidently, Timoshenko design techniques are necessary when designing resonators with frequencies in the upper VHF range

Temperature Dependence.

Because they are virtually levitated above the silicon substrate, and thus should be nearly impervious to the structure-to substrate thermal expansion mismatches that plague clamped-clamped beam resonators, one might expect the described free-free beam resonators to exhibit smaller thermal dependencies than their clamped-clamped beam counterparts. To test this assumption, modifications were made to the custom-built vac-

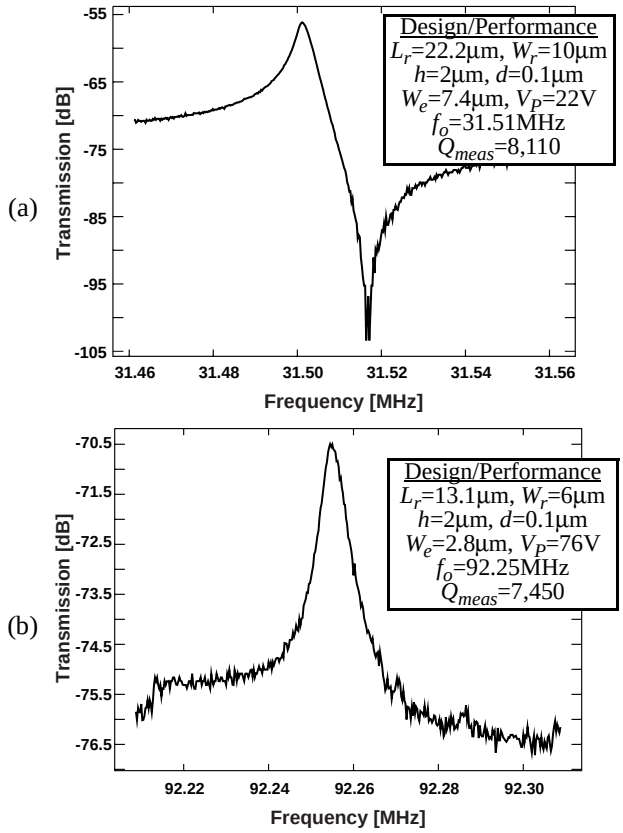

Fig. 11: Measured spectra for (a) a 31.51MHz free-free beam μresonator; and (b) a 92.25 MHz free-free beam μresonator.

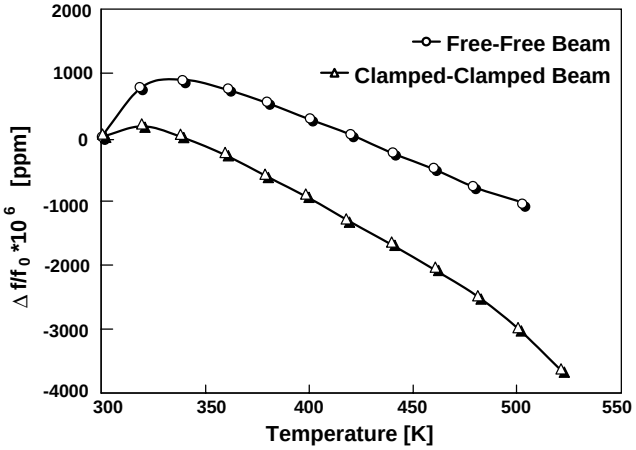

Fig. 12: Fractional frequency versus temperature plots for a clamped-clamped beam and a free-free beam μmechanical resonator.

uum chamber to allow insertion of an MMR Technologies temperature-controllable cantilever, enabling measurement of the temperature dependence of resonator center frequencies [12].

Figure 12 presents measured plots of fractional frequency change versus temperature for a 53.6MHz free-free beam μmechanical resonator and a 4.2MHz clamped-clamped beam lateral μmechanical resonator. From the linear regions of the curves, the extracted temperature coefficients are 12.5ppm/^{o}C and 16.7ppm/^{o}C for the free-free and clamped-clamped versions, respectively. Although the free-free beam does show slightly better performance, the degree of improvement is not as large as might be expected. One possible reason for this may be that the stiffness of these high frequency resonators is so large—on the order of 54,000N/m—that stiffness changes due to thermal expansion stresses are now insignificant in comparison, and thus, have less influence on the thermal stability of f_o.

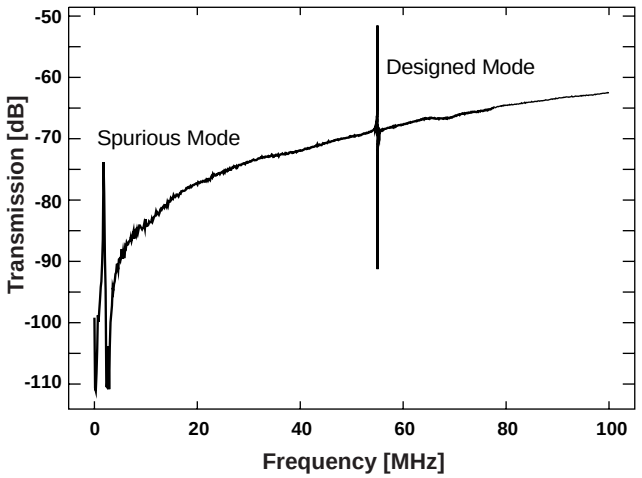

Fig. 13: Frequency characteristic for a 55MHz free-free beam μmechanical resonator measured over a wide frequency range in search of spurious responses.

Figure 12 not only provides thermal stability information, it also elucidates an important issue concerning micro-scale devices: susceptibility to contamination. In particular, the peaked curves seen in Fig. 12, where frequency initially rises with temperature then drops past a certain threshold temperature, can be explained by a mass-removal based model, where contaminants are burned or evaporated off the resonator surfaces as temperatures increase, removing excess mass, and initially raising the frequency of the resonator. When all contaminants are removed, the frequency increase ceases, and the expected decrease in frequency with temperature (due to a negative Young's modulus temperature coefficient) is then observed. Given that typical micromechanical resonator masses are on the order of 10^{-13} kg, such a model is quite plausible, and even expected, even under the high vacuum environment used to obtain Fig. 12. Admittedly, however, the vacuum achieved in our custom chamber may have lacked sufficient purity, especially given out-gassing from inserted circuit boards. For this reason, vacuum encapsulation at the wafer- or package-level is being investigated as a means to alleviate the observed contamination phenomena.

Spurious Responses.

Although very effective for maximizing the *Q* of μmechanical resonators, the described free-free beam design does exhibit one important drawback in that its more complex design leads to spurious modes. Such modes, if not suppressed or moved to distant frequencies, can interfere with the performance of filters or oscillators utilizing this resonator design. Figure 13 presents the frequency characteristic for a 55MHz free-free beam μmechanical resonator measured over a wide frequency range, from 1kHz to 100MHz, in search of spurious modes. One spurious mode is observed at 1.7 MHz, which is sufficiently far from the desired frequency (55MHz) to be rendered insignificant for many applications. If not far enough, modifications to the supports can be made to move this peak even further away, or damping strategies based on low *Q* filtering or support material modifications can be used to remove the peak entirely.

It should be mentioned that a rather excessive amount of parasitic feedthrough is observed in the wide range measurement of Fig. 13, and this feedthrough becomes especially troublesome past 90MHz. Shielding measures at both the board and the substrate levels are planned to alleviate this feedthrough component for future measurement of even higher frequency resonators.

VI. CONCLUSIONS

Using a combination of quarter-wavelength torsional supports attached at node points and electrically-activated, dimple-determined electrode-to-resonator gaps, the free-free beam μmechanical resonator design demonstrated in this work adeptly removes the anchor dissipation and processing problems that presently hinder their clamped-clamped beam counterparts, and in doing so, successfully extends the application range of high-*Q* microelectromechanical systems to the mid-VHF range, with plenty of *Q* to spare en route to even higher frequencies. The present μmechanical resonator design achieves *Q*'s exceeding 8,000 in a frequency range that includes some of the most popular IF's used in many cellular and cordless communication sub-systems, and does so while retaining the high stiffness needed to maintain adequate dynamic range in both oscillator and filtering applications.

The VHF frequencies demonstrated in this work by no means represent the ultimate range of μmechanical resonator technology, especially given that the observed *Q* of this design seems to maintain its high value throughout the designed range of frequencies, showing little or no roll-off with increasing frequency. Needless to say, research towards UHF and beyond continues.

Acknowledgments: The authors are grateful for fabrication support from Qing Bai, and testing support from Hao Ding (who measured the 70MHz clamped-clamped μbeam spectrum). This work was supported by DARPA under Agreement No. F30602-97-2-0101, with portions supported by NSF and NASA/JPL.

References

[1] C. T.-C. Nguyen, "Micromachining technologies for miniaturized communication devices (invited)," *Proceedings* of SPIE: Micromachining and Microfabrication, Santa Clara, California, Sept. 20-22, 1998, pp. 24-38.

[2] F. D. Bannon III, J. R. Clark, and C. T.-C. Nguyen, "High frequency microelectromechanical IF filters," *Technical Digest*, 1996 IEEE Electron Devices Meeting, San Francisco, CA, Dec. 8-11, 1996, pp. 773-776.

[3] A.-C. Wong, H. Ding, and C. T.-C. Nguyen, "Micromechanical mixer+filters," to be published in the *Technical Digest*, IEEE International Electron Devices Meeting, San Francisco, California, Dec. 6-9, 1998.

[4] C. T.-C. Nguyen, "Frequency-selective MEMS for miniaturized communication devices (invited)," *Proceedings, 1*998 IEEE Aerospace Conference, Snowmass, Colorado, March 21-28, 1998, pp. 445-460.

[5] W. T. Thomson, *Theory of Vibration with Applications*. New Jersey: Prentice-Hall, 1981.

[6] S. Timoshenko, *Strength of Materials, Part I: Elementary Theory and Problems, 3rd Ed.* Malabar: Krieger Pub. Co., 1958.

[7] H. Nathanson, W. E. Newell, R. A. Wickstrom, and J. R. Davis, Jr., "The resonant gate transistor," *IEEE Trans. Electron Devices*, vol. ED-14, No. 3, pp. 117-133, March 1967.

[8] W. C. Tang, T.-C. H. Nguyen, and R. T. Howe, "Laterally driven polysilicon resonant microstructures," *Sensors and Actuators*, **20**, 25-32, 1989.

[9] W. E. Newell, "Miniaturization of tuning forks," *Science*, vol. 161, pp. 1320-1326, Sept. 1968.

[10] C. T.-C. Nguyen and R. T. Howe, "An integrated CMOS micromechanical resonator high-*Q* oscillator," to be published in *IEEE J. of Solid-State Circuits*, April 1999.

[11] K. Wang and C. T.-C. Nguyen, "High-order micromechanical electronic filters," *Proceedings*, 1997 IEEE International Micro Electro Mechanical Systems Workshop, Nagoya, Japan, Jan. 26-30, 1997, pp. 25-30.

[12] W.-T. Hsu and C. T.-C. Nguyen, "Geometric Stress Compensation for Enhanced Thermal Stability in Micromechanical Resonators," to be published in the *Proceedings* of the 1998 IEEE International Ultrasonics Symposium, Sendai, Japan, Oct. 5-8, 1998.